Investigation on Particle Self-Assembly in Solid Lipid–Based Colloidal Drug Carrier Systems

Andreas Illing,[1,4] Tobias Unruh,[2] Michel H. J. Koch[3]

Received December 15, 2003; accepted January 9, 2004

Purpose. The effect of spontaneous particle self-assembly into stack-like structures occurring in dispersions of melt-homogenized tripalmitin nanocrystals (solid lipid nanoparticles; SLNs) was studied in dependence of lipid concentration, stabilizer type, stabilizer concentration, and particle size.

Methods. Tripalmitin nanosuspensions with concentrations ranging from 20 to 200 mg/g were prepared by high-pressure melt homogenization. The formulations were characterized by synchrotron small-angle X-ray scattering (SAXS), photon correlation spectroscopy (PCS), and freeze-fracture transmission electron microscopy (TEM).

Results. Dispersions of partly self-assembled particles could be derived both with anionic or cationic surfactants. Particle self-assemblies were observed in such formulations when the tripalmitin concentration exceeds 40 mg/g. Further increase of the lipid concentration enhances particle self-assembly. The tendency to form self-assemblies is also influenced by the particle shape. The interparticle distances in stacked lamellae are determined by the tripalmitin concentration and by the surfactant concentration.

Conclusions. Parallel alignment of tripalmitin nanoplatelets is a completely reversible and concentration-dependent effect that can be attributed to the overlap of the exclusion volumes of the anisometric particles. The usefulness of this effect might be explored for the formulation of drug delivery systems.

KEY WORDS: nanoparticles; particle self-assembly; small-angle X-ray scattering; stacked lamellae; tripalmitin.

INTRODUCTION

Aqueous dispersions of crystalline, tripalmitin nanoparticles (solid lipid nanoparticles; SLNs) are being investigated as novel carrier systems e.g., for dermal, peroral, and parenteral administration of drugs. Such formulations might increase the bioavailability of drugs and enable sustained release or even site-specific drug delivery (1–3).

To characterize the physical state as well as the size and shape of dispersed nanosized lipid carriers under *in situ* conditions, small-angle X-ray scattering (SAXS) has succesfully been used in different cases (4–7). Recent studies on dispersions of platelet-shaped trimyristin and tripalmitin nanoparticles, however, revealed unexpected scattering features in the small-angle region, which can be interpreted as the first, second, third, and so forth, order of a single interference, corresponding to a repeat unit of approximately 35 nm (8). Because such spacings are too large for triglyceride crystal lattice structures, the interference has been attributed to the self-assembly of particles forming stacked lamellae (8) (Fig. 1). The existence of such ordered structures was confirmed by transmission electron microscopy (TEM), and they have been found to correspond to isolated stacks of up to 10 particles floating in an isotropic particle dispersion.

In the current study, we investigated in detail the formation of stacked lamellae in triglyceride formulations by SAXS and TEM. The formation of stacked lamellae may accelerate formulation instabilities, such as gelation and particle growth, and also have an impact on the rheological behavior of the formulations. It is, therefore, of pharmaceutical relevance to ascertain the relationship between formulation parameters and the formation of such stacked lamellae in order to optimize the physical properties of the dispersions in view of future medical application.

MATERIALS AND METHODS

Triglyceride nanosuspensions were produced by high-pressure melt homogenization: a mixture of tripalmitin (TP; Dynasan 116, Condea AG, D-Witten, Germany) and soybean phospholipid (P; Lipoid S100, Lipoid KG, D-Ludwigshafen, Germany) was melted at 80°C. Simultaneously, a solution of sodium glycocholate (GC; Sigma, D-Steinheim, Germany) or cetylpyridinium chloride (CP; Caesar & Loretz, D-Hilden, Germany) in purified water containing 22.5 mg/g glycerol was heated to 80°C. The aqueous solution was added to the lipid, and a preemulsion was prepared using a high-speed stirring device (Ultra-Turrax, Jahnke & Kunkel, D-Staufen, Germany). The crude emulsion was subsequently passed through a heated (85°C) high-pressure homogenizer (Micron Lab 40, APV Gaulin, D-Lübeck, Germany) usually for four times at 1200 bar and once at 1500 bar. To crystallize the lipid, the emulsions were allowed to cool to room temperature and were finally stored in sealed 20-ml vials ($T \approx 8$°C). Details on the applied sample compositions are displayed in Table I. Particle concentration increase after manufacturing was achieved by ultrafiltration using a Millipore stirred cell (Millipore, D-Eschborn, Germany). Part of the aqueous phase was separated using a membrane of regenerated cellulose (molecular mass cutoff: 30,000 Da) applying a pressure of approximately 2 bar.

Particle size (z-average) and particle size distribution (polydispersity index) of each formulation were determined within 1 day after preparation using photon correlation spectroscopy (PCS, Zeta Plus, Brookhaven Instruments, Holtsville, NY, USA). Dispersions were analyzed after appropriate dilution with dust-free water, and particle sizes were calculated applying the cumulant method. Because this algorithm is based on the assumption of spherical particles, the z-average values do not represent a real extension of the platelet-like particles, but characterize the dispersions by a mass proportional value of the most frequent particles. Typical z-averages (polydispersity indices) are 140 nm (0.17) for GC and 160 nm (0.17) for CP samples.

Determination of the amount of free, not adsorbed, CP in the aqueous phase of the samples was performed by measuring the light absorption at a wavelength of 259 nm (photometer DU146, Beckman, D-Krefeld, Germany) after removing the tripalmitin particles by ultrafiltration (method as described above).

[1] Friedrich Schiller University Jena, Institute of Pharmacy, Department of Pharmaceutical Technology, D-07743 Jena, Germany.
[2] Technical University Munich, ZWE, FRM-II, D-85747 Garching, Germany.
[3] European Molecular Biology Laboratory, Hamburg Outstation, D-22603 Hamburg, Germany.
[4] To whom correspondence should be addressed. (e-mail: andreas.illing@uni-jena.de)

0724-8741/04/0400-0592/0 © 2004 Plenum Publishing Corporation

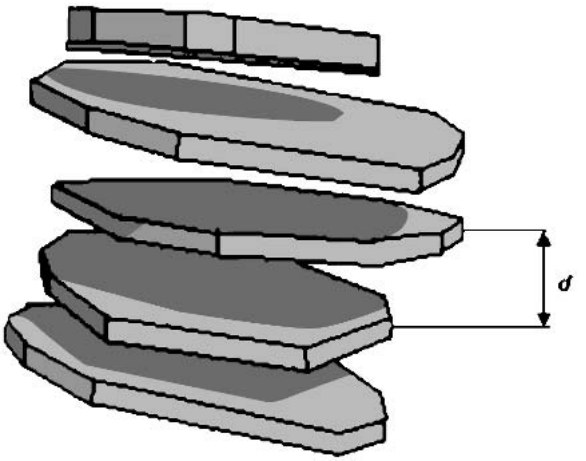

Fig. 1. Schematic representation of a single stack consisting of five self-associated tripalmitin nanocrystals (*d*: length of a repeat unit = particle thickness plus interparticle distance).

SAXS was performed using the X33 double-focusing small-angle camera of the European Molecular Biology Laboratory (EMBL) (9) on the DORIS III storage ring of the Deutsches Elektronensynchrotron (DESY; D-Hamburg, Germany). Samples of about 100 μl each were filled in a sample holder, thermostated at 25°C, and positioned in the beam. Data were recorded in at least 10 independent 1-min time frames at *s*-values between 0.02 nm^{-1} and 0.4 nm^{-1} ($s = 2 \sin \theta/\lambda$) using a quadrant or linear gas proportional detector (10) with delay line readout with either a time to digital converter (11) or a module implementing space–time–space conversion (12).

Electron micrographs were taken using a CEM 902A transmission electron microscope (Zeiss, D-Oberkochen, Germany) operating at 80 kV. Samples were frozen as thin films in liquid propane, freeze fractured at 173 K and 5×10^{-6} mbar (BAF400, Bal-Tec, Liechtenstein), and shadowed with platinum/carbon at 45°. The replicas were mechanically stabilized by vertical deposition of pure carbon.

SAXS-DATA TREATMENT

For each measurement, the patterns of all 1-min time frames were checked for sample stability, and all time frames passing this check were averaged. Those raw data were corrected for detector response using the homogeneous scattering pattern of an iron foil. Background was subtracted in order to achieve a horizontal baseline. The abscissa of the diffraction patterns was scaled using second to eleventh orders of a collagen standard sample ($d = 64.5$ nm). (Note: Data treatment was performed using the *embl2xy* program available from T. Unruh.)

SAXS patterns of highly concentrated tripalmitin dispersion exhibit typically, besides the broadened (001) Bragg reflection of the tripalmitin β-modification at $s \approx 0.235$ nm^{-1}, several almost equidistant interference maxima at lower *s*-values. These maxima are the higher orders of interference due to the stacked arrangement of platelet-like particles (stacked lamellae) within the dispersions. Partially, they superimpose on the Bragg reflection resulting in a more or less strong distortion of this peak.

The scattering pattern thus results from the superposition of two contributions. The dominating one is that of isolated tripalmitin nanocrystals (I_{NC}) with a weight fraction $(1 - x)$ close to unity. The second one corresponds to the spherically averaged contribution of the weight fraction x of nanocrystals in stacked lamellae, I_{SL}, which in first approximation is the product of the scattering of individual nanocrystals, assumed to be spherical at low resolution, and of an interference function representing the stacks (S).

$$I(s) = (1 - x)I_{NC}(s) + xI_{NC}(s)S(s). \tag{1}$$

It should thus in principle be possible to establish the degree of stack formation from the ratio

$$\frac{I(s)}{I_{NC}(s)} = (1 - x) + xS(s) = 1 + x[S(s) - 1] \tag{2}$$

where $I_{NC}(s)$ is the scattering of the corresponding stack-free dilution of the same sample.

Two important structural parameters of the stacked lamellae should thus be extractable from the scattering curves: (i) the average of a repeat distance d between the particles' centers of mass, and (ii) the fraction of self-associated particles, as described below.

In practice, the ratio in Eq. (2) is too noisy at higher *s*-values to apply this procedure with confidence, and another approach was therefore followed. The experimental SAXS curves were fitted using Pearson VII functions with a Marquardt–Levenberg least square method (Fig. 2) to determine

Table I. Sample Compositions and Homogenization Parameters

Tripalmitin content (mg/g)	Lecithin content (mg/g)	Costabilizer content (CP or GC) (mg/g)	Homogenization parameters
20	4.8	1.2, 6	4 × 1200 + 1 × 1500 bar
40	9.6	2.4, 6	4 × 1200 + 1 × 1500 bar
60	14.4	3.6, 6	4 × 1200 + 1 × 1500 bar
80	19.2	4.8, 6	4 × 1200 + 1 × 1500 bar
100	24	2, 4, 6, 8, 10, 15	4 × 1200 + 1 × 1500 bar
		6	5 × 500 bar
			5 × 800 bar
			4 × 1000 bar
			4 × 1500 + 1 × 1600 bar
150	36	6, 9	4 × 1200 + 1 × 1500 bar
200	48	6, 12	4 × 1200 + 1 × 1500 bar

CP, cetylpyridinium; GC, glycocholate.

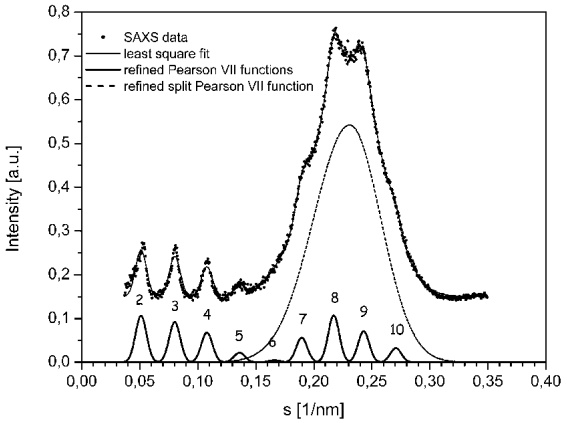

Fig. 2. Background subtracted SAXS pattern of a P/CP–stabilized dispersion containing 100 mg/g TP. The experimental data were fitted to a combination of nine refined Pearson VII functions representing the stack-related interferences and one refined split Pearson VII function representing the (001)-Bragg reflection. The numbers mark the order of the corresponding interference maximum. Experimental data and the least square fit are shifted vertically by 0.15 for better visualization.

the *s*-values of the interference maxima due to the stacked lamellae and separately that of the (001) Bragg reflection.

The d_n-values obtained from the *n*th order interferences ($d_n = n/s_n$) deviate by up to 5 nm from strict equidistance due to the effect of the underlying scattering of the tripalmitin nanocrystals. Comparison with the ratio in Eq. (2) in the region where it is meaningful indicates, however, that the parameter $\bar{d} = \sum_{n \in M} dn/N$ (M, set of all observable, stack-related interference maxima; N, number of all observable, stack-related interference maxima) gives an accurate value for the spacing.

For the determination of the degree of particle self-association, proportionality between the experimentally measured intensity of the stack-related interferences and the total number of platelets assembled into stacks is assumed. Thus, we define a relative degree of stack formation (δ_{rel}) as:

$$\delta_{rel} = \frac{\int I_S}{\int I_S + \int I_B} \times 100\% \qquad (3)$$

where $\int I_S$ is accumulated integrated intensity of all stack-related interferences and $\int I_B$ is integrated intensity of the (001) Bragg reflection of the tripalmitin crystal structure.

For the calculation of the integrated intensity, the refined peak functions were used. δ_{rel} is, therefore, a semiquantitative measure for the fraction of platelets organized in stacked lamellae. It should be noted that δ_{rel} yields, however, neither information on the number of stacks in a dispersion nor information on the number of particles in a single stack.

Because the lowest accessible *s*-value in the SAXS experiments was 0.02 nm^{-1}, the first interference maximum could not be detected. The missing contribution of this reflection will lead to deviations in the absolute value of δ_{rel}, but the error will approximately be proportional to the absolute value itself.

RESULTS AND DISCUSSION

In order to study the influence of TP concentration on the extent of stack formation, a series of seven TP formulations in the concentration range from 20 to 200 mg/g were produced following the method described above. In all formulations, a constant ratio TP:P:CP (or TP:P:GC) = 100:24:6 was kept. In Fig. 3, the relative degrees of stack formation, as derived from SAXS data analysis, are displayed as a function of TP content. Formulations with 20 and 40 mg/g TP do not display stack-related interferences ($\delta_{rel} = 0$). For more concentrated dispersions (from 60 to 200 mg/g), which all exhibit the interferences, a linear dependence between TP concentration and δ_{rel} was found. A second series of dispersions covering the same concentration range was prepared simply by dilution of the 200 or 150 mg/g TP formulations with appropriate amounts of aqueous phase. As illustrated in Fig. 3, these formulations exhibit essentially the same δ_{rel}-values as equally concentrated native dispersions. Finally, and as a third way of adjusting the concentration, the native 20 and 40 mg/g dispersions were concentrated by ultrafiltration to a TP concentration of about 100 mg/g. After this procedure, the formulations exhibit stack-related interference patterns, in contrast to the original dispersions. These experiments clearly indicate that particle self-assembly does not depend on the preparation technique. Within experimental error, it is completely reversible and depends on the concentration of the disperse phase. Obviously, there exists a threshold of about 40 mg/g TP (or about 50 mg/g total lipid) that has to be exceeded for inducing a significant stack formation.

Some dispersions were investigated by TEM to visualize the particle self-assemblies (Figs. 4a and 4b). The images exhibit in each case very thin, polygonal nanocrystals that are partially assembled into stacked lamellae. The stacks consist of almost parallely oriented particles with a rather narrow size distribution. Larger particles appear to have a greater tendency to associate, whereas smaller particles are less frequently found in stacked lamellae. In dispersions of high TP content, the fraction of particles arranged in stacked lamellae is obviously higher than in less concentrated samples. This observation agrees with the results of the SAXS experiments. The stacks in most samples are sharply defined, comparatively small objects with sizes below 500 nm. In 150 and 200 mg/g TP samples, the stacks even form three-dimensional domains.

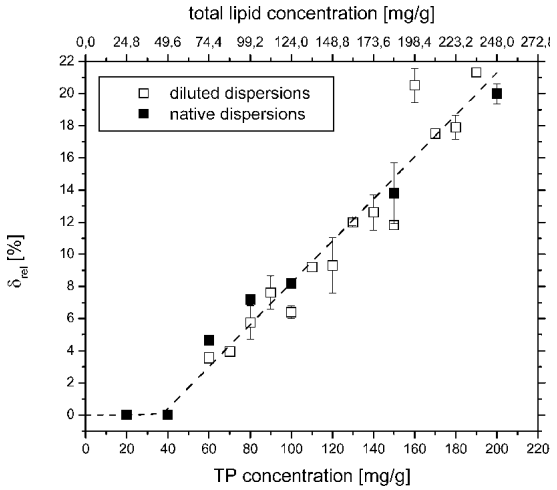

Fig. 3. Effect of total lipid concentration and TP concentration on δ_{rel} in P/CP–stabilized samples with equal TP:P:CP ratio.

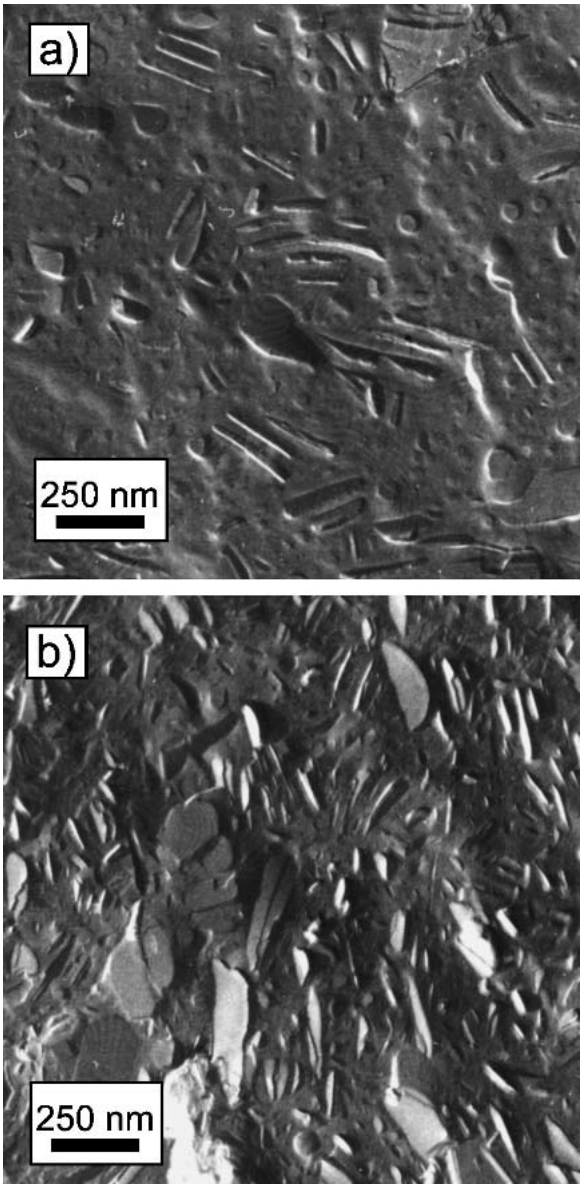

Fig. 4. Freeze-fracture electron micrographs of CP-stabilized TP nanosuspensions containing (a) 80 mg/g TP and (b) 200 mg/g TP, respectively.

The observation of local close packing of nanocrystals in moderately concentrated dispersions leads to the assumption that steric restrictions of particle movement cause the formation of stacked lamellae. This effect can be estimated as described in the following.

TP nanocrystals are highly anisometric and can roughly be approximated by flat cylinders. Free rotational movement of such particles requires a much larger, spherical volume (exclusion volume) than the actual volume of a particle itself. The exclusion volume fraction of all suspended particles (φ), under the condition of $D >> h$, is given by

$$\varphi = V_{ex} \cdot N = V_{ex} \frac{\varphi_{disp}}{V_{cyl}} = \frac{1}{6} \pi D^3 \cdot \frac{4\varphi_{disp}}{\pi D^2 h} = \frac{2}{3} \frac{D}{h} \varphi_{disp} \qquad (4)$$

where V_{ex} is exclusion volume of a single particle, N is number of particles in a given volume, φ_{disp} is volume fraction of the disperse phase, V_{cyl} is volume of a single particle, D is particle diameter, and h is particle thickness. Adsorption of the ionic surfactants on the surface of the particles causes electrostatic repulsion between the platelets and further increases the exclusion volume. This effect can be considered in Eq. (4) by introducing a correction term leading to Eq. 5 (13):

$$\varphi = \frac{2}{3} \frac{D}{h} \left(1 + \frac{2\lambda_d}{D}\right)^3 \varphi_{disp} \qquad (5)$$

with λ_d being the Debye screening length ($\lambda_d = 1/\kappa$, wher κ ισ Hückel parameter). At a certain critical volume fraction of the dispersed phase (φ^*) the exclusion volumes of the individual particles overlap, as the closest packing of spherical exclusion volumes (74% volume fraction) is reached:

$$\varphi = 0.74 = \frac{2}{3} \frac{D}{h} \left(1 + \frac{2\lambda_d}{D}\right)^3 \varphi^*. \qquad (6)$$

This critical volume fraction (φ^*), in analogy to Ref. 14, is given by:

$$\varphi^* = 0.74 \left(\frac{3}{2}\right) \left(\frac{h}{D}\right) \frac{1}{\left(1 + \frac{2\lambda_d}{D}\right)}. \qquad (7)$$

For volume fractions exceeding this threshold, not all particles can move freely anymore, and, consequently, some will be forced into a denser arrangement. A further increase of the particle concentration leads to more stacked particles. Electrostatic repulsion forces, which distribute evenly over the particle surfaces, cause the parallel arrangement of the platelets.

From TEM images, the mean aspect ratio D/h of the platelets has roughly been estimated to be between 12 and 15 [h = 15 nm (8), $180 \leq D \leq 225$ nm]. Assuming a λ_d value of 2 nm, Eq. (7) yields φ^*-values of between 0.07 and 0.09 or concentrations of disperse phase between 70 and 90 mg/g [disperse phase: TP plus P, ρ_{B-TP} = 1039 kg·m^{-3}; (15)]. These values are in fairly good agreement with the threshold derived from SAXS data analysis (between 50 and 60 mg/g disperse phase; Fig. 3).

The observation of particle self-assembly and the attribution to an exclusion volume effect is in full agreement with earlier computer simulations on disk-like hard-core particles performed by Veerman and Frenkel (16), which predicted the formation of short columns of platelets in low concentrated isotropic phases (for $D/h = 15 \rightarrow \varphi < 0.15$) and its enhancement at higher particle number densities.

Figure 5 displays background corrected scattering patterns of 100 mg/g TP dispersions stabilized with P and GC. These formulations have been prepared by applying different homogenization pressures and vary only in their mean particle sizes, but not in their composition. Interestingly, the intensities of the stack-related interferences depend significantly on the mean particle sizes. The finest dispersion exhibits well resolved peaks and the coarsest dispersion almost none. For D/h = constant and $D >> \lambda_d$, Eq. 7 predicts an almost constant φ^*-value. Therefore, we interpret the effect as resulting from a size-dependent decrease in the D/h ratio that consequently will shift the φ^* to values above 100 mg/g TP. Actually, the scattering patterns of the coarse dispersions exhibit significantly narrower (001) peaks than the finer dis-

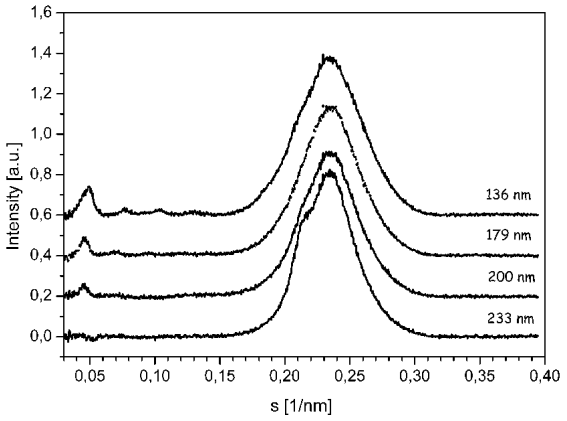

Fig. 5. Background-subtracted SAXS curves of P/GC–stabilized TP dispersions (100 mg/g) varying in the mean particle size (PCS *z*-average) as indicated. The curves are slightly smoothed and shifted vertically for better visualization.

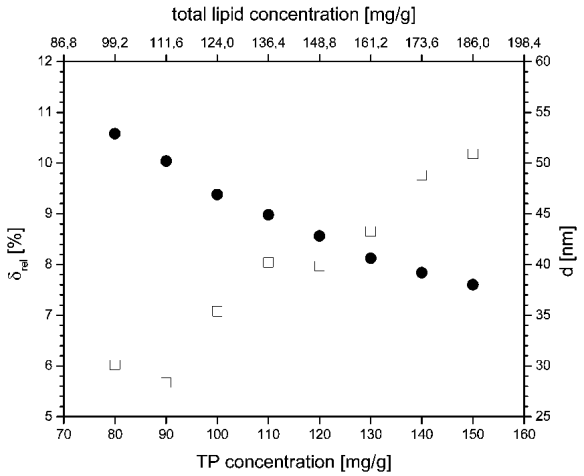

Fig. 7. Effect of TP concentration on δ_{rel} and the average repeat length *d* in formulations with constant CP concentration (6 mg/g). Squares (□) indicate δ_{rel}-values; points (●) indicate repeat units.

persions indicating a strong increase in the particles dimension perpendicular to the (001) plane (= thickness *h*). Furthermore, the scattering curves of the 200-nm and the 233-nm particles exhibit weak shoulders at $s \approx 0.215$ nm^{-1}, indicating residues of the TP α-modification. For such α-TP particles, a more spherical shape than that observed with β-TP particles has been described earlier (17).

The influence of costabilizer concentration on stack formation has been examined using a series of five 100 mg/g TP dispersions stabilized with 24 mg/g P and between 2 and 10 mg/g CP (Fig. 6). Due to the constant TP concentration in all samples, the δ_{rel}-values only vary within experimental error, but the repeat distance *d* decreases significantly from 52 to 38 nm with increasing CP concentration. Therefore, it seems that the costabilizer concentration determines the distances between the self-assembled nanocrystals. In Fig. 7, however, it is displayed that also at a constant CP concentration (6 mg/g), the repeat distances change, if only the TP concentration of the sample is varied. Figure 8 presents the *d*-values of dispersions with similar TP content as in Fig. 7, but with different CP concentrations. The repeat distances *d*, likewise, decrease with increasing TP concentration. Comparison of both diagrams yields almost no differences in *d* for the two dispersions of equal TP content. It must be assumed, therefore, that in the last two cases, the costabilizer concentration has only a minor influence on the interparticle distances, which are, like the fraction of self-assembled particles, mainly dominated by the particle concentration. Only in the case of constant particle content and strongly different concentrations does the influence of the costabilizer become prominent. The detected decrease of *d* with increasing costabilizer content seems surprising, as increasing amounts of adsorbed ionic surfactant on the particles' surface should enhance interparticle electrostatic repulsion. Determination of the CP concentration in the dispersion medium of such TP/CP systems indicates, however, not only an increase in the amount of adsorbed surfactant, but also an increase in the concentration of free CP in an almost constant ratio of about 99:1. Therefore, a reasonable explanation for the lower *d*-values might be the enhanced screening of electrostatic repulsion due to an increasing ionic strength in the dispersion medium.

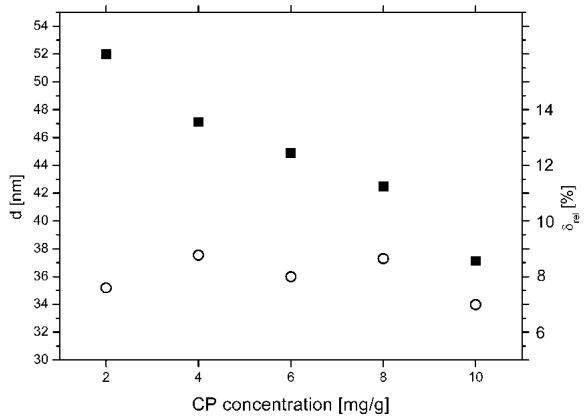

Fig. 6. Effect of CP concentration and δ_{rel} and the mean length of a repeat unit *d* in native formulations with constant TP concentration (100 mg/g). Points (○) indicate δ_{rel}-values; squares (■) indicate repeat units.

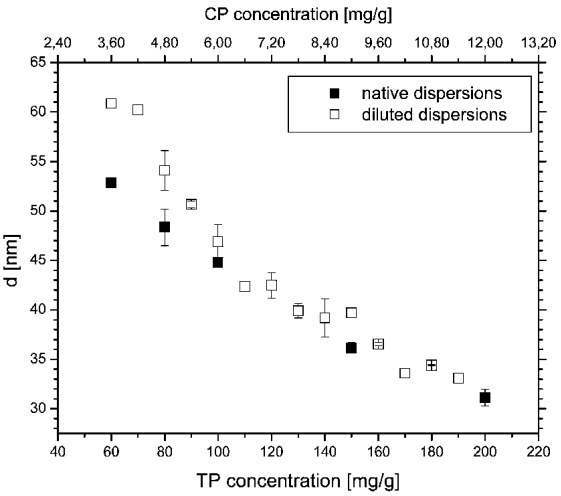

Fig. 8. Effect of concentration on the average repeat length *d* in stacked lamellae in different P/CP–stabilized samples with equal TP:P:CP ratio.

CONCLUSIONS

It has been shown by small-angle X-ray scattering that the self-assembly of dispersed triglyceride nanocrystals into stacked lamellae is an entirely reversible and concentration-dependent process. The phenomenon can be attributed to steric restrictions of the movement of strongly anisometric particles. By changing the triglyceride concentration and the mean particle size, it is possible to control the concentration of stacked lamellae in a reproducible manner. To some extent also, the nature and concentration of ionic costabilizers, besides the triglyceride content, influence the interparticle distances, most notably by electrostatic effects.

No indications were found for accelerated instabilities of the examined formulations due to particle self-assembly. With only few exceptions, the dispersions were stable for at least 2 years. Therefore, stack formation seems not to have a negative influence on the pharmaceutical quality of triglyceride nanosuspensions.

The use of stacked lamellae as a new type of carrier system for the administration of drugs has been proposed earlier (8). The basic idea is to intercalate drug substances in the interparticle gaps and thus to achieve a protection of the drug against enzymatic degradation or even a modified release behavior. The current investigations, however, demonstrate a rapid dissociation of drug-free stacked lamellae upon dilution, as would occur upon administration, for example, into the bloodstream. Nevertheless, in some cases it should be possible to stabilize stacked lamellae by cross-linking them via strongly surface-attached macromolecules, such as peptides or nucleic acids, and thus to obtain injectable composite particles with sizes well below 1 μm.

ACKNOWLEDGMENTS

The authors thank S. Richter, Jena, for preparation of freeze-fracture samples and for taking the electron micrographs. Financial support was granted by the European Community—Access to Research Infrastructure Action of the Improving Human Potential Program to the EMBL Hamburg Outstation (Contract No. HPRI-CT-1999-00017).

REFERENCES

1. K. Westesen and B. Siekmann. Biodegradable colloidal drug carrier systems based on solid lipids. In S. Benita (ed.), *Microencapsulation*, Marcel Dekker, New York, 1996, pp. 213–258.
2. K. Westesen. Novel lipid-based colloidal dispersions as potential drug administration systems—expectations and reality. *Colloid Polym. Sci.* **278**:608–618 (2000).
3. R. H. Müller, K. Mäder, and S. Gohla. Solid lipid nanoparticles (SLN) for controlled drug delivery—a review of the state of art. *Eur. J. Pharm. Biopharm.* **50**:161–177 (2000).
4. K. Westesen, B. Siekmann, and M. H. J. Koch. Investigation on the physical state of lipid nanoparticles by synchrotron radiation X-ray diffraction. *Int. J. Pharm.* **93**:189–199 (1993).
5. W. Schütze and C. C. Müller-Goymann. Phase transformation of a liposomal dispersion into a micellar solution induced by drug-loading. *Pharm. Res.* **15**:538–543 (1998).
6. H. Bunjes, M. H. J. Koch, and K. Westesen. Effect of particle size on colloidal solid triglycerides. *Langmuir* **16**:5234–5241 (2000).
7. G. Lukowski, J. Kasbohm, P. Pflegel, A. Illing, and H. Wulff. Crystallographic investigation of cetylpalmitate solid lipid nanoparticles. *Int. J. Pharm.* **196**:201–205 (2000).
8. T. Unruh, K. Westesen, P. Boesecke, P. Lindner, and M. H. J. Koch. Self-assembly of triglyceride nanocrystals in suspension. *Langmuir* **18**:1796–1800 (2002).
9. M. H. J. Koch, I. Bordas. X-ray diffraction and scattering on disordered systems using synchrotron radiation. *Nucl. Instrum. Meth.* **208**:461-469 (1983).
10. C. J. Boulin, R. Kempf, A. Gabriel, and M. H. J. Koch. Data acquisition-systems for linear and area x-ray-detectors using delay-line readout. *Nucl. Instrum. Meth.* **A269**:312–320 (1988).
11. A. Gabriel. Position-sensitive x-ray detector. *Rev. Sci. Instrum.* **48**:1303–1305 (1977).
12. C. deRaad Iseli. T. Reimann, F. Golding, C. Boulin, A. Epstein, E. Beloeuvre, A. Gabriel, and M. H. J. Koch. A data acquisition system for gas proportional detectors with delay line readout based on space-time-space conversion. *Nucl. Instrum. Meth.* **A467**:1152–1155 (2001).
13. R. J. Hunter. *Foundations of Colloid Science*, Vol. II, Clarendon Press, Oxford, 1989, pp 827–834.
14. S. Jogun and C. F. Zukoski. Rheology of dense suspensions of plateletlike particles. *J. Rheol.* **40**:1211–1232 (1996).
15. A. van Langevelde, K. van Maalsen, F. Hollander, R. Peschar, and H. Schenk. Structure of mono-acid even-numbered β-triacylglycerols. *Acta Cryst.* **B55**:114–122 (1999).
16. J. A. C. Veerman and D. Frenkel. Phase behavior of disklike hard-core mesogens. *Phys. Rev. A* **45**:5632–5648 (1992).
17. H. Bunjes, M. H. J. Koch, and K. Westesen. Influence of emulsifiers on the crystallization of solid lipid nanoparticles. *J. Pharm. Sci.* **92**:1509–1520 (2003).